Jet Grout Slab to Reduce Wall Movements Caused by Excavation

L.W. Wong
SMEC Asia Limited, Hong Kong

doi: https://doi.org/10.21467/proceedings.7.7.20

ABSTRACT

Two-dimensional numerical analysis has been conducted on an excavation case in soft ground using jet grout slab to reduce wall deflections. The Young's moduli of the jet grout slab were assessed from the uniaxial compression tests with the axial strains ranging from 0.4 % to 1.4 %. The lower bound secant moduli and uniaxial compressive strengths for the jet grout slab have been adopted in the numerical analysis. The computed wall deflections and ground movements match with those observed in the inclinometers installed in wall and in ground. The analyzed results show that the jet grout slab is an effective measure that could reduce the wall deflections by 36 %. By using the wall deflection path concept, the effects of the jet grout slab and adjacent piles on the wall movements have been assessed in a convenient way.

Keywords: Jet grout slab, Hardening-Soil Model, Small Strain, Wall deflection path.

1 INTRODUCTION

Jet grouting has been one of the strengthening measures for reducing wall deflections of deep excavations in soft clay. Buried struts by means of jet grout slabs are often installed below the final excavation level aiming to reduce the maximum wall deflections occurring at that level. In numerical analysis, estimation of the stiffnesses of the jet grouted soil has been one of the challenges to the professional. The uniaxial compressive strengths of the jet grouted soil scatter in wide range. Secondly, like the soil materials, the cement grouted soil mass is non-linear and exhibits strain-softening at the post-peak strain levels. The post-peaks uniaxial compressive strengths would be as low as 10 % of the peak values. The performance of excavations supported by the jet grout slab shall be closely monitored to check if the wall movements would encroach to the post-peak range.

In this paper numerical analysis has been conducted on an excavation case history on City Hall Station supported with jet grout slab. The Hardening-Soil with Small Strain stiffness (HSS) model has been adopted for the soft clay. For the jet grout slab, the Hardened-soil (HS) model has been adopted. The wall deflection path concept has been adopted to assess the effects of the jet grout slab and the adjacent piles on reduction in wall deflections. Further than that, the abrupt change in the rate of wall deflection indicating the nonlinear performance of the jet grout slab could be readily identified in the wall deflection paths. The result of analysis is presented herein to provide a rational approach for design and assessment on the effects of the jet grout slab in reducing wall deflections.

2 CASE HISTORY ON JET GROUTING

2.1 Excavation case at City Hall Station

City Hall Station of the Nankang Line, Taipei MRT, is located in the K1 Geological Zone (MAA, 1987) at the eastern portion of the Taipei Basin. The excavation case history was presented by Chen et al. (1997). As depicted in Figure 1 and Figure 6, the station is 278 m in length and 24 m in width. The subsoil is mainly composed of a clay stratum of 43 m in thickness. The excavation was carried out to a depth of 18.8 m.

Proceedings DOI: 10.21467/proceedings.7.7; Series: AIJR Proceedings; ISSN: 2582-3922; ISBN: 978-81-989164-3-3

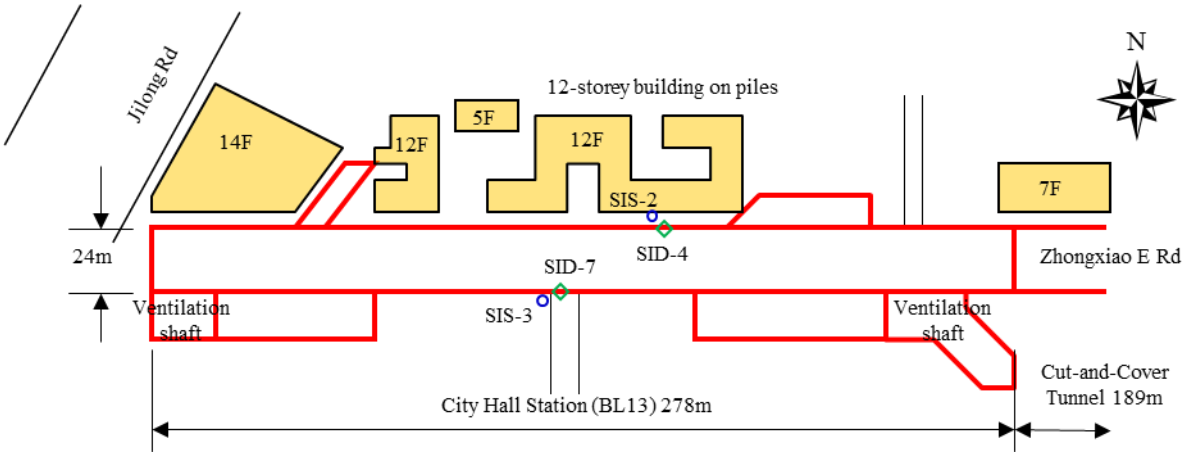

Figure 1: Instrumentation layout of the City Hall Station

The pit was retained by diaphragm wall of 1.2 m in thickness and 45 m in length. The excavation in 6 stages was supported by 5 levels of steel struts. Inclinometers SID4, SID7, SIS2 and SIS3 were deployed on both sides of the station. According to Chen at al. (1997), it was estimated that the wall deflections for the excavation in soft clay supporting with the diaphragm wall of 1.2 m in thickness would be as large as 75 mm. The ground settlements would then exceed the allowable limits. As there were existing buildings of 7-storey to 14-storey located on the north side of the station, jet grout slab of 4 m in thickness was installed beneath the final excavation level to reduce the wall deflections and the ground movements. The jet grout slab was installed during the period between April 1994 and November 1994. Excavation commenced in January 1995. The final excavation depth of 18.8 m was reached in June 1995 and the base slab was cast in September 1995.

2.2 Groundwater conditions

The piezometric level in the Jingmei Formation, a gravel (GM) layer, was lowered to a level near the bottom of the Songshan Formation in the 1970s due to excessive extraction of groundwater to supply water to the city, leading to significant reductions in water pressures in the Songshan Formation and substantial ground settlements as a result. The piezometric level in the Jingmei Formation did not recover till 1974 although pumping had been banned since 1968. The subsoils in the Songshan Formation in the Taipei Basin are thus substantially over-consolidated. Based on monitoring records at the deep well at Sun Yet Sin Memorial Hall, located at 0.5 km west of City Hall Station, Hwang & Moh (2022) reported that the piezometric level in the Jingmei Formation in the eastern portion of the Taipei Basin was around El. -10.0 m in 1995. In the central portion of the Taipei Basin, the piezometric level in the Jingmei Formation recovered to El. 0 m in 2017.

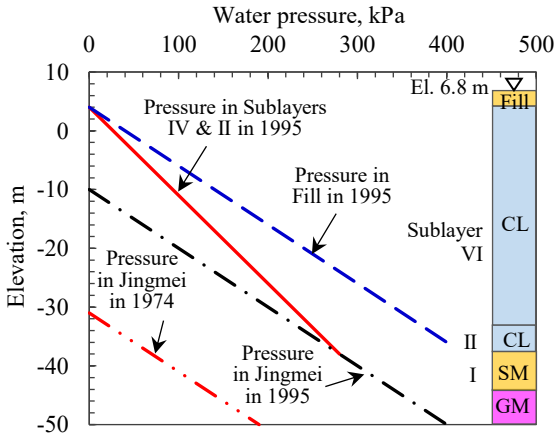

Figure 2: Groundwater pressures on the outer face of the diaphragm walls

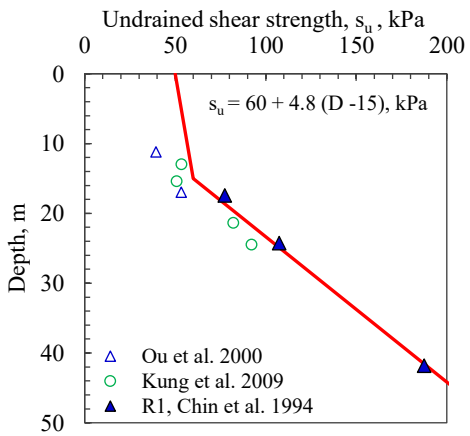

Figure 3: Undrained shear strengths of clays obtained by CK_0UC triaxial tests (after Wong 2024a)

The distributions of the water pressures outside the diaphragm wall at City Hall Station in 1995 are presented in Figure 2. For the Sublayer I and the Jingmei Formation, the piezometric level of El. -10.0 m in 1995 is adopted. The water pressures for Sublayers II to IV clay (CL) are interpolated between the fill layer and Sublayer I sand (SM). Inside the pit, the piezometric levels maintaining at a depth of 1 m below the excavation levels in each stage have been adopted in the analysis.

2.3 Undrained shears strengths for clay sublayers

The undrained shear strengths of the clayey Songshan Formation obtained by the Ko consolidated compression undrained tests were reported by Chin et al. (1994), Ou et al. (2000) and Kung et al. (2009). The undrained shear strength profile is presented in Figure 3. Based on these test results, Wong (2024a) determined that the undrained shear strengths of the Sublayers IV and II clayey soils at the depths below 15 m in the K1 Geological Zone of the Songshan Formation could be expressed by the empirical Equation 1:

$$s_u = 60 + 4.8\ (D - 15) \text{ in kPa} \tag{1}$$

where D is the depth in metre and s_u is the undrained shear strength in kPa.

3 CHARACTERISTICS OF JET GROUTED SOIL

3.1 Peak strength and secant modulus

The properties of the jet grout slab installed at City Hall Station was reported by Wong & Hwang (1997). The jet grout slab was installed by Jumbo Special Grout, the double-fluid JSG method. The jet grout piles were 2.55 m in diameter spacing at 2.2 m in triangular pattern. As presented in Figure 4, the uniaxial compressive strengths, σ_p, of the core specimens taken from the jet grout slab ranged from 1.8 MPa to 9.4 MPa, with an average of 3.8 MPa. The secant moduli, the E_{50} values interpreted at 50 % σ_p, ranged from 0.11 GPa to 0.38 GPa.

In-situ pressuremeter (PMT) tests were performed in the jet grout slabs. The PMT tests indicated that the σ_p values ranged from 0.8 MPa to 4.8 MPa, with an average of 2.4 MPa. It is noted that two of the PMT tests had the undrained shear strength $s_{u\text{-}pmt}$ values of 30 kPa and 90 kPa, which are virtually the untreated soil strength.

The E_{50} values are commonly normalized with the σ_p values of the jet grouted soil. Figure 5 shows the relationship between the E_{50}/σ_p ratios and the axial strains occurring at 50 % σ_p, the ε_{50} values. Based on the 60 number of the uniaxial compression tests reported by Wong & Hwang (1997), regression analysis gives the relationship that expressed in Equation 2:

$$E_{50} / \sigma_p = 0.5 / \varepsilon_{50} \tag{2}$$

Equation 2 is exactly the definition of the secant modulus of the jet grouted soil. The E_{50}/σ_p ratios are inversely proportional to the axial strains, the ε_{50} values.

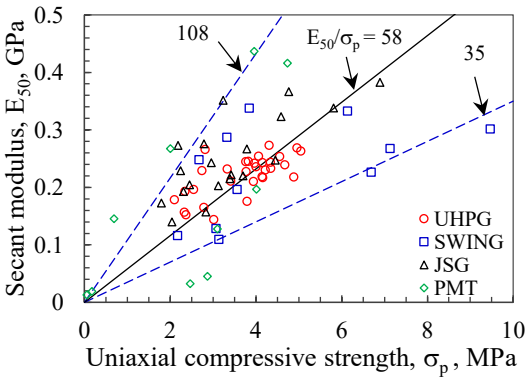

Figure 4: Uniaxial compressive strengths versus secant moduli of jet grouted soil (after Wong & Hwang 1997)

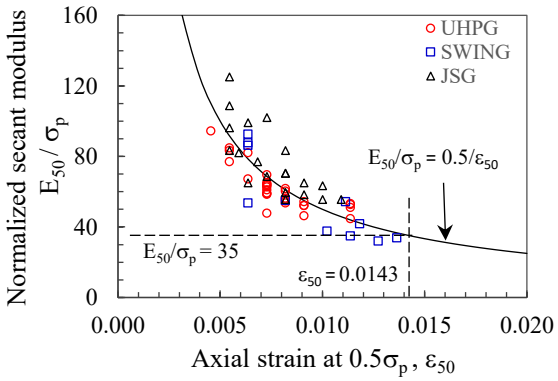

Figure 5: Variation of secant moduli with axial strains for jet grouted specimens

Proceedings DOI: 10.21467/proceedings.7.7
ISBN: 978-81-989164-3-3

Series: AIJR Proceedings
ISSN: 2582-3922

Figure 4 shows that the E_{50}/σ_p ratios of the jet grouted soil ranged from 35 to 108, with an average of 58. According to Equation 2, the ε_{50} values for the UCS tests ranged from 0.4 % to 1.4 % with an average of 0.86 %. The widely scattering in the E_{50}/σ_p ratios in Figure 4 are caused by the variation in ε_{50} values mobilizing the 50 % σ_p.

3.2 Modeling of the jet grout slab

Based on the results of uniaxial compression tests conducted on 90 core specimen of jet grouted soil, Wong (2024b) reported that the stress-strain relationship of the jet grouted soil is nonlinear. The moduli defined at the peak strengths, E_p, are lower than those for the secant moduli, E_{50}. The E_{50}/E_p ratio is around 1.4. In this numerical analysis, the Hardening-soil (HS) model is adopted for simulating the nonlinearity of the jet grouted soil. The stiffness parameters for inputting the HS model are given in Equations (3) and (4):

$$E^{ref}_{50} = E^{ref}_{oed} = E_{50} \quad (3)$$

$$E^{ref}_{ur} = 2.8\ E^{ref}_{50} \quad (4)$$

where E^{ref}_{ur} , E^{ref}_{50} and E^{ref}_{oed} are the reference stiffness parameters for the HS model and E_{50} is the secant moduli for the jet grouted soil obtained by the UCS tests. In this analysis, the lower bound E_{50}/σ_p ratio of 35 presented in Figure 5 is adopted. Using a σ_p value of 1 MPa, the E^{ref}_{ur} value of 100 MPa computed by Equations (3) and (4) is adopted in the numerical analysis.

4 NUMERICAL SIMULATIONS

4.1 Finite element mesh

The 2-Dimensional finite element model for the numerical analysis is depicted in Figure 6. The width of the excavation is 24 m. The excavation is carried out to a depth of 18.8 m in the analysis. The lateral extent of the finite element model reaches a distance of 100 m from the central axis of the excavation trench. The ground model is 60 m in depth. The diaphragm wall of 45 m in length is located at a distance of 12 m from the axis of the trench. The Jingmei Formation is a competent formation with very high stiffness. However, the base of the finite element model in this study is placed at a depth of 60 m to include a 9 m layer of the Jingmei Formation to ensure that the contribution of this formation to ground movements is accounted for.

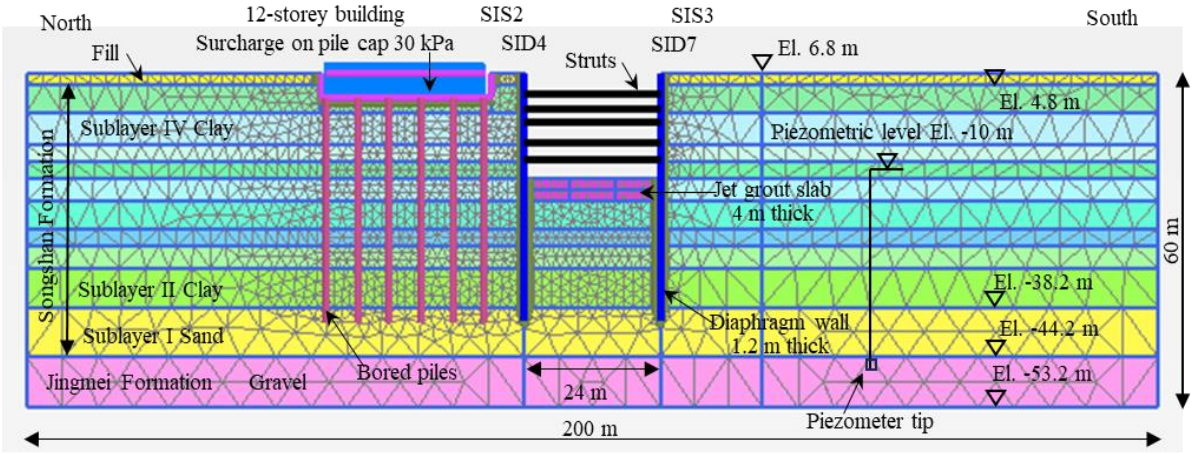

Figure 6: Finite element mesh for the analytical section for 6 stages of excavation

4.2 Hardening-soil with small-strain stiffness model for the surrounding ground

The PLAXIS-2D finite element software developed by PLAXIS BV (2013) has become a very popular tool in geotechnical analysis and design. The Hardening-Soil with Small-strain stiffness (HSS) constitutive soil model is an extension of the Hardening-Soil (HS) model (Benz 2006, Schanz & Vermeer 1998; Schanz et al. 1999)

introduced in the PLAXIS program and is adopted herein to simulate the non-linear stress-strain relationship of soils under loading and unloading conditions.

Wong (2024a) adopted the HSS soil model in the study for the effect of diaphragm wall installation to ground movements for City Hall Station. The stiffness parameters adopted for the various soil layers are presented in Table 1. The Readers can refer to that reference for the relationship of the stiffness parameters with the undrained shear strengths and with the N values. The effective shear strength parameters, i.e., the c' and ϕ' values, for the silty sand strata, are determined from laboratory tests conducted on thin-wall tube specimens.

It is noted that for the clayey layers, c' = s_u and $\phi' = 0^o$ is assumed in the analyses. The dilation angle, ψ', of 2^o, 0^o, and 3^o are adopted for the sandy, the clayey, and the gravelly soils respectively. The R_f equals 0.9 is adopted. The unload-reload Poisson's ratio, υ_{ur}, of 0.2 is used as suggested by Benz (2006) and Schanz et al. (1999). Although the HSS soil model is an effective stress model and adopting the $\phi' = 0^o$ for the clayey soils loses its compression hardening function and stress-dependent stiffness, parametric studies using both the effective and the total stress models show that the computed wall deflections and settlements are essentially the same. The total stress model for clay is adopted in this study.

In the PLAXIS software, an elastic-plastic model following the Mohr-Coulomb criterion is used to describe the interfaces for the soil-structure interaction. The R_{inter} value of 1 is the rigid mode and represents the rough interface. In this study, the R_{inter} value of 0.7 has been adopted for the soil-wall interface and along the interface between the wall and the jet grout slab.

Table 1: Soil parameters for the HSS model adopted in the PLAXIS analyses

Mid depth m	Soil type	Unit weight γ' kN/m^3	N value	Undrained shear strength s_u, kPa	Effective cohesion c' kPa	Effective friction angle ϕ', deg	Dilation angle ψ' deg	Reference stiffness, MPa		Initial shear moduli G^{ref}_0, MPa
								Secant stiffness E^{ref}_{50}	Unload-reload stiffness E^{ref}_{ur}, MPa	
1	SM	18.5	8	-		30	0	16	80	80
4.5	CL	18.4	2	54	0			8.1	41	41
10	CL	18.4	3	57				8.6	43	43
14.5	CL	18.4	4	60				9	45	45
17.5	CL	18.4	5	72				10.7	54	54
20.5	CL	18.4	6	88				13.2	66	66
25.5	CL	19	7	110				16.5	82	82
29.5	CL	19	9	130				19.5	97	97
33	CL	19.5	10	146	0			22	110	110
38.55	CL	19.5	20	173				26	130	130
46.5	SM	19.5	26	-	0	32	2	52	260	260
55.5	GM	21.9	>100	-	0	35	3	200	1000	1000

4.3 Determination of small-strain stiffness of soil

The parameters for the small-strain stiffness, i.e., the G^{ref}_0 and the $\gamma_{0.7}$, have been determined from the laboratory tests. Based on the results of the bender element tests, Kung et al. (2009) obtained the G_{max}/s_u ratios ranging from 738 to 788, with an average ratio of 759 for the axial compression tests, where G_{max} is the initial shear modulus. For the axial extension tests, the G_{max}/s_u ratios ranged from 614 to 751, with an average of 671. In this study, the $G^{ref}_0 = 750\ s_u$ is adopted.

Chin et al. (2007) presented the CK_0UDSS test results that depicted in Figure 7. Santos & Correia (2001) recommended that the stress-strain curve for small-strains can be described in Equation 5 as:

$$G / G_0 = 1 / (1+ 0.385\ \gamma / \gamma_{0.7}) \quad (5)$$

where G_0 is the maximum small-strain shear modulus. The moduli degradation curves with the threshold $\gamma_{0.7}$ values ranging from 0.8×10^{-4} to 10^{-3} are shown in Figure 8. The degradation of the shear moduli with shear strain interpreted from the direct simple shear test is presented Figure 8, showing that the Taipei clay would have the $\gamma_{0.7}$ value of 5×10^{-4}. This $\gamma_{0.7}$ value has been adopted in this study.

Proceedings DOI: 10.21467/proceedings.7.7
ISBN: 978-81-989164-3-3

Series: AIJR Proceedings
ISSN: 2582-3922

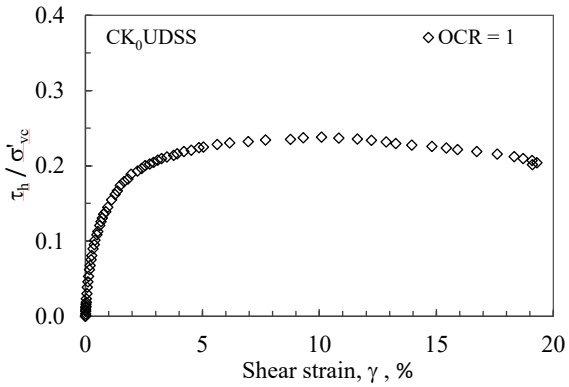

Figure 7: Stress-strain curve of Taipei clay under CK_0UDSS test (After Chin et al. 2007)

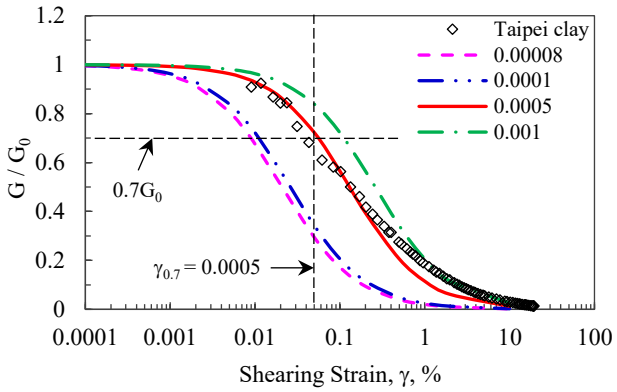

Figure 8: Degradation of shear moduli with shearing strain (after Wong 2024a)

4.4 Modeling of the retaining structures and piles

The excavation scheme and the retaining structures for City Hall Station are depicted in Figure 6. The diaphragm wall is simulated by plate element and an E_c value of 25,000 MPa is adopted for concrete with a characteristic compressive strength of 28 MPa. The estimated flexural rigidity (denoted as E_cI_c where I_c is the moment of inertia) and the axial stiffness (denoted as E_cA_c where A_c is the sectional area) of the diaphragm wall of 1.2 m in thickness are 2,520 MN-m and 21,000 MN/m respectively. These values have already been reduced from their original values by 30 % to account for tensile cracks and creeping of concrete during excavation.

The excavation was supported by 5 levels of steel struts, which are represented by the node-to-node anchors. The properties for the steel struts are presented in Table 2. The Young's modulus (E_s) for steel of 210 GPa has been adopted. The struts had the horizontal spacing, s, of 4.5 m. The 50 % design preloads have been adopted to cater for releasing of the strut loads caused by loading of the adjacent struts.

As shown in Figures 1 and 6, there is a 12-storey building supported on bored piles on the north side of City Hall Station. Chen et al. (1999) reported that the concrete bored piles were 0.8 m to 1.2 m in diameter and 45 m in depth. There was one basement floor at 4.5 m depth. The building load of 30 kPa acting at the basement level has been adopted in the analysis.

The embedded beam model available in the PLAXIS software is adopted to simulate the piles. The embedded beam is a 2.5-Dimensional model taking the stiffnesses of the pile and the surrounding soil into account. In this study the pile diameter of 0.85 m spacing at 5.5 m along the east-west direction have been adopted. The Young's modulus of 18,000 MPa for the concrete piles is used. Sensitivity analysis on the effect of the pile stiffness using one-half of the AE value found that the effects to wall movements are insignificant.

Table 2: Strut properties

Excavation stage	Strut level	Depth of strut, m	Strut type	Area A_s, cm^2	Stiffness E_sA_s/s, MN/m	Design preload, kN/m
1	S1	3.8	1H300x300x10x15	138.5	645	120
2	S2	6.4	1H400x400x13x21	218.7	1,021	150
3	S3	9.0	1H350x350x12x19	347.8	1,623	250
4	S4	12.2	2H400x400x13x21	437.4	2,041	255
5	S5	15.4	2H400x400x13x21	437.4	2,041	255

4.5 Analysis cases

Three cases have been analyzed to assess the performance of the jet grout slab and its effectiveness on reducing wall deflections. Case 1 considered the jet grout slab of 4 m in thickness. Case 2 assessed the performance of the jet grout slab of 2 m in thickness. The jet grout slab is located at the depths between 18.8 m and 20.8 m. Case 3 analyzed the conditions without the jet grout slab. Table 3 summarizes the features for these analytical cases.

5 RESULTS OF NUMERICAL ANALYSIS

5.1 Computed versus observed wall deflections

The computed wall deflection profiles for Case 1 with the 4 m thick jet grout slab are presented in Figure 9 and Figure 10. The analysis results are compared with those observed in the inclinometers installed on the north and the south sides of the station. Inclinometers SIS4 and SID7 were installed in the diaphragm wall. Inclinometers SIS-2 and SIS-3 were installed in ground at the distance of 2 m behind the diaphragm walls. The toe levels of the diaphragm walls were at 45 m depth. The toe levels of the inclinometers on the north side, SID4 and SIS2, were at 49.5 m depth. For SID7 and SIS4 installed on the south side, their toe levels were at 48.0 m depth.

As shown in Figure 9 and Figure 10, the computed wall deflection profiles in the final stage fall between those observed in wall and in ground. The deviation between the computed and the observed profiles have been less than 1 mm. In the intermediate Stage 4, Figures 9b and 10b show that the computed maximum deflections deviate by 6 mm at the north wall and by 9 mm at the south wall. The discrepancies could be attributable to various conditions and are discussed in Section 6.3.

Comparison of the wall deflections between the north and the south sides shows that with the presence of the piles, the maximum computed wall deflections of 32.4 mm for the north wall have been less than the 42.3 mm that computed for the south wall.

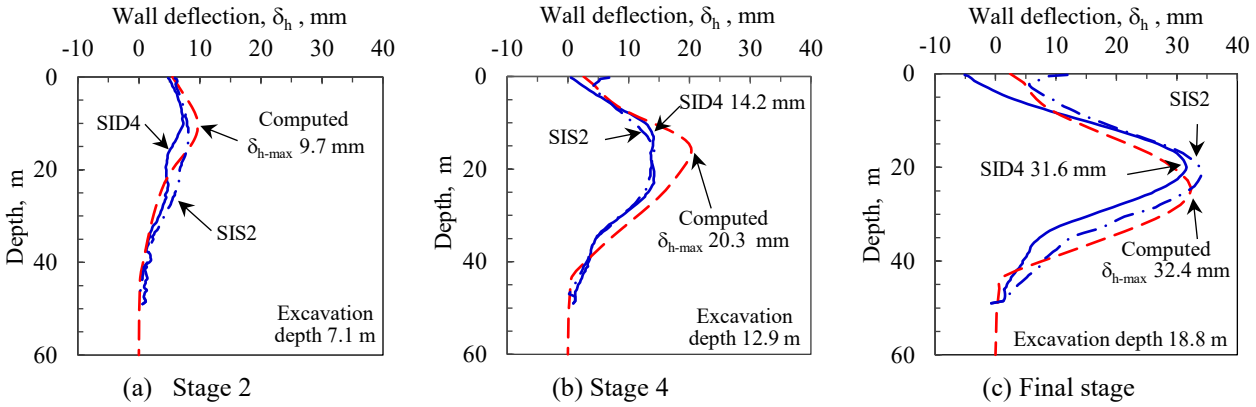

Figure 9: Computed and observed wall deflections at north wall with piles nearby - Case 1

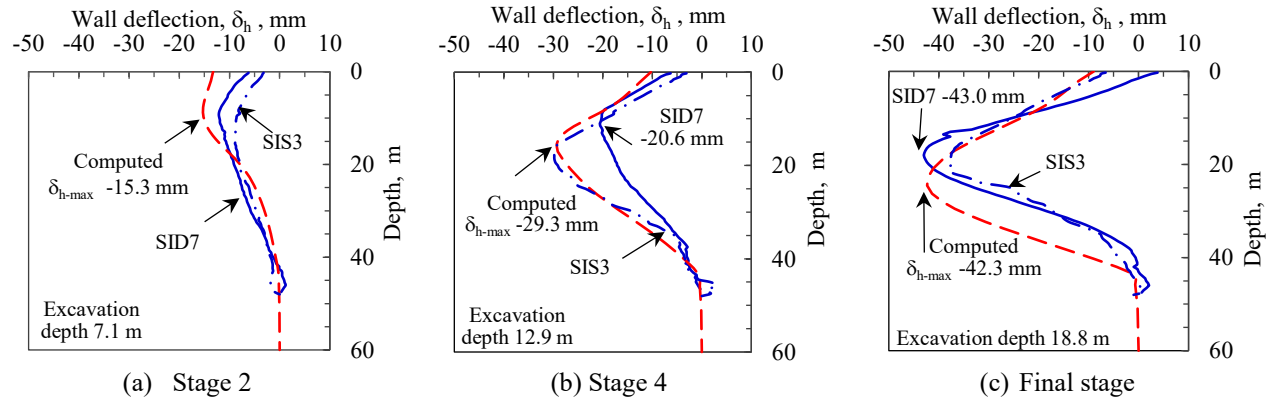

Figure 10: Computed and observed wall deflections at south wall with no pile - Case 1

5.2 Effects of jet grout slab and piles

The computed wall deflection profiles for Case 1 to Case 3 in the final stage are presented in Figure 11. As summarized in Table 3, the deflections were affected by the jet grout slab and by the piles. For the south wall with no pile, the maximum wall deflections in Case 1 with 4 m thick jet grout slab could be reduced by 36 %, from 66.3 mm to 42.3 mm. For Case 2 with 2 m thick jet grout slab, the wall deflections could be reduced by

Proceedings DOI: 10.21467/proceedings.7.7
ISBN: 978-81-989164-3-3

Series: AIJR Proceedings
ISSN: 2582-3922

22 %, from 66.3 mm to 51.6 mm. Comparing the deflections between the north and the south walls, the presence of the piles next to the north wall could reduce the wall deflections by around 23 % in Case 1 to Case 3.

Prakasa & Hsiung (2023) reported the results of numerical analysis on the jet grout slab conducted at Yung Chun Station (BL14), which is located at 1 km east of City Hall Station (BL13). The excavation of 16.7 m in depth and 19.5 m in width was supported with diaphragm wall of 38 m in length and 1.2 m in thickness. With the jet grout slab of 3 m in thickness, the maximum wall deflection could be reduced by 33 %, from 39 mm to 26 mm. That 33 % reduction is similar to the 36 % reduction computed at the south wall of City Hall Station.

Table 3: Effects of piles and jet grout slab to wall deflections in the final stage

Case	Feature	Computed maximum wall deflection		Effects of piles $\delta_{h\text{-}N}/\delta_{h\text{-}S}$	Effects of jet grout slab	
		North side with piles, $\delta_{h\text{-}N}$, mm	South side with no pile, $\delta_{h\text{-}S}$, mm		North	South
Case 1	Jet grout slab 4 m thick	32.4	-42.3	0.77	0.62	0.64
Case 2	Jet grout slab 2 m thick	39.5	-51.9	0.76	0.76	0.78
Case 3	No jet grout slab	51.9	-66.3	0.78	1	1

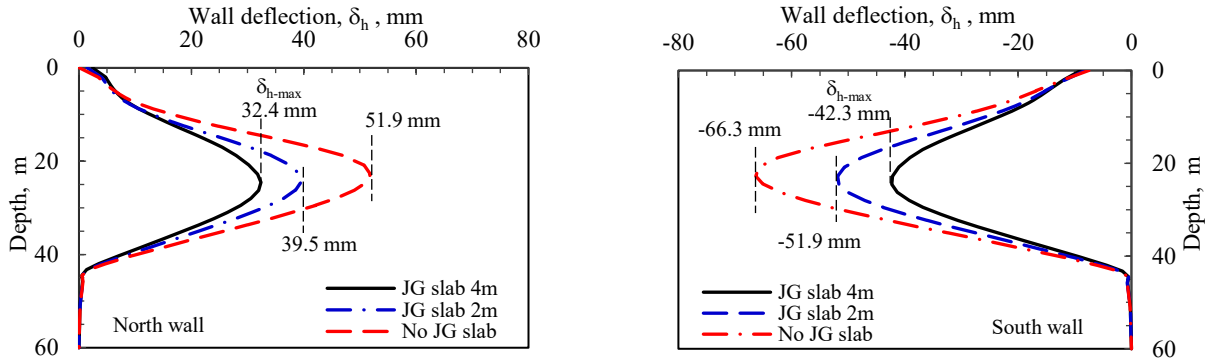

(a) North wall with piles nearby (b) South wall with no pile

Figure 11: Computed wall deflections in the final stage with and without jet grout slab - Case 1 to Case 3

5.3 Axial strains in the jet grout slab

The computed axial strains along the top, the middle and the bottom levels, or at the depths of 18.8 m, 20.8 m and at 22.8 m, of the jet grout slab in the final stage for Case 1 are presented in Figure 12a. Along the middle level the jet grout slab would have the horizontal strains, ε_h, ranging from -0.09 % to -0.36%, with an average of -0.29 %. The largest ε_h value of -1.20 % occurred at the top corners, at the interface between the walls and the jet grout slab. The localized strains concentration is compatible with the upper range of axial strain of 1.4 % for the jet grout slab that shown in Figure 5. It is noted that the negative value denotes compressive strain.

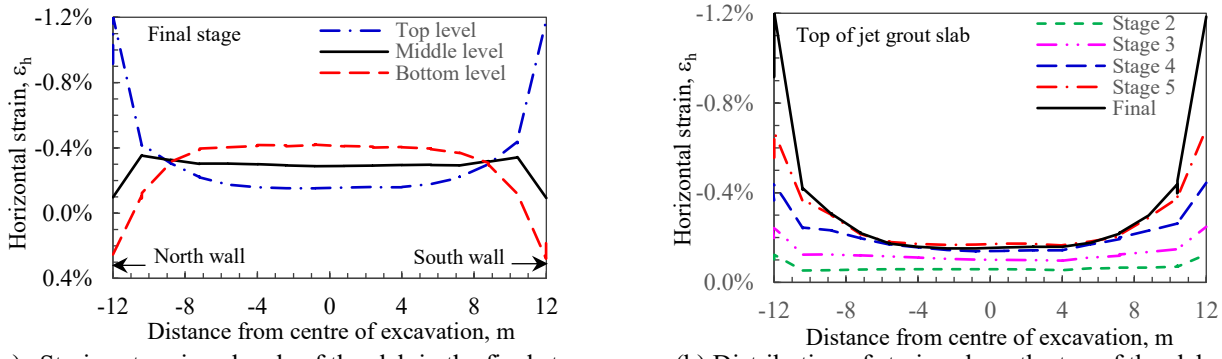

(a) Strains at various levels of the slab in the final stage (b) Distribution of strains along the top of the slab

Figure 12: Computed horizontal strains along the jet grout slab in various stages - Case 1

Figure 12b shows the development of the ε_h values at the upper corners of the jet grout slab. The computed maximum ε_h values in Stages 3, 4, 5 and in the final stage have been -0.25 %, -0.44 %, -0.68 % and -1.20 % respectively. The abrupt increase in the ε_h values from -0.68 % to -1.2 % between Stage 5 and the final stage is likely due to the nonlinear response of the jet grout slab in the final stage.

Figure 12a shows that the axial strains along the central portion of the jet grout slab in the final stage range from -0.2 % to -0.4 %. As these axial strains are less than the lower bound strain of 0.4 % shown in Figure 5, majority of the jet grout slab has not encroached to the post-peak range. The use of the HS model for simulating the jet grout slab is applicable in this study.

5.4 Back-analyzed stiffnesses for the jet grout slab

The parameters of E^{ref}_{ur} of 100 MPa, E^{ref}_{50} of 35 MPa and the σ_p value of 1 MPa for the jet grout slab have been obtained by back-estimation in this study. According to Chen et al. (1997), the minimum σ_p value of 1.2 MPa was specified for the jet grout slab at City Hall Station. The back-calculated σ_p value of 1 MPa is close to the specified minimum value. It is noted that the UCS tests were conducted on good quality core specimens and inferior specimens could not be taken for testing. As the in-situ tests could detect weak seams in the jet grouted soil mass, it would be prudent to conduct more pressuremeter tests to determine the σ_p values to be adopted for future jet grout slabs design and analysis.

6 ASSESSMENTS ON THE PERFORMANCE BY WALL DEFLECTION PATHS

6.1 Effects of piles

The assessment on the effects of the jet grout slab to wall deflections in Table 3 compared only the results in the final stage. The wall deflections in all stage are also useful information for assessing the performance. Moh & Hwang (2005) adopted the wall deflection path concept to assess the performance of the excavation cases. The deflection path is basically plotting of the maximum wall deflections against the excavation depths in various stages. Expressed in log-log scale, the wall deflection path falls into a common straight line under the similar hydro-geological conditions. The wall deflection path is defined by Δ_4 and Δ_{100}, where Δ_4 is the maximum wall deflections occurring at the excavation depth within 4 m and Δ_{100} is the projection of the maximum wall deflection values from the 4 m depth to the excavation depth of 100 m.

The application of the wall deflection path is demonstrated in Figure 13. The computed maximum wall deflections versus the excavation depths for Case 3 with no jet grout slab from Stage 1 to the final stage are plotted up in Figure 13. The Δ_4 values of 6 mm and 10 mm respectively are interpreted for the north and the south walls. The Δ_{100} value 500 mm is interpreted both for the north and the south walls. The presence of the piles on the north side only affects the wall deflections at shallow depths. As excavation goes deeper, the effects of piles diminish so that the Δ_{100} value is unaffected. The piles next to the wall had the effects of reducing the Δ_4 values by 40 %, from 10 mm to 6 mm.

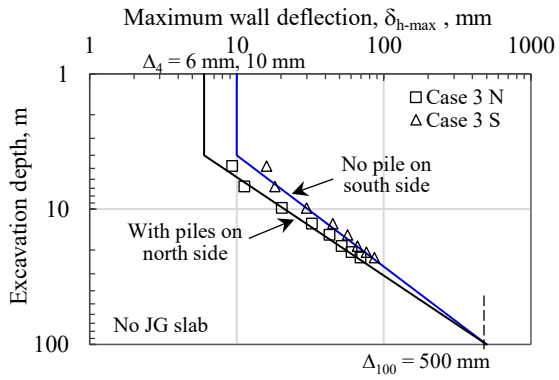

Figure 13: Effects of piles assessed by wall deflection paths - Case 3

Proceedings DOI: 10.21467/proceedings.7.7
ISBN: 978-81-989164-3-3

Series: AIJR Proceedings
ISSN: 2582-3922

The set of the Δ_4 and the Δ_{100} values of 10 mm and 500 mm respectively for the south wall with no jet grout slab and no pile nearby is consistent with that for the excavation cases in the K1 Geological Zone of the Taipei Basin, which is dominant with thick deposits of soft clay. Hwang et al. (2016) proposed that the reference deflection path for the diaphragm wall of 1.0 m in thickness and 15 m to 25 m in excavation width could be defined with the Δ_4 and the Δ_{100} values of 10 mm and 500 mm respectively.

6.2 Effects of jet grout slab

Figure 14 shows the wall deflection paths for the cases with and without the jet grout slab, Case 1 and Case 3. For the north wall next to the piles, the deflection path with the Δ_4 and Δ_{100} values of 6 mm and 200 mm respectively is interpreted for Case 1 in Figure 14a. For the south wall with no pile nearby, the deflection path with the Δ_4 and the Δ_{100} values of 10 mm and 200 mm respectively is interpreted for Case 1 in Figure 14b.

The wall deflection paths for Case 3 presented in Figure 13 are reproduced in Figure 14 for comparison with those for Case 1. The effects of the jet grout slab to the north and the south walls are discernable. Figure 14 shows that for the walls on both sides, the presence of the jet grout slab reduces the Δ_{100} values from 500 mm to 200 mm. As the excavation goes deeper, the effectiveness of the jet grout slab increases. Figure 14 also shows that the jet grout slab has minimal influence on shallow excavation so that the Δ_4 value is unaffected.

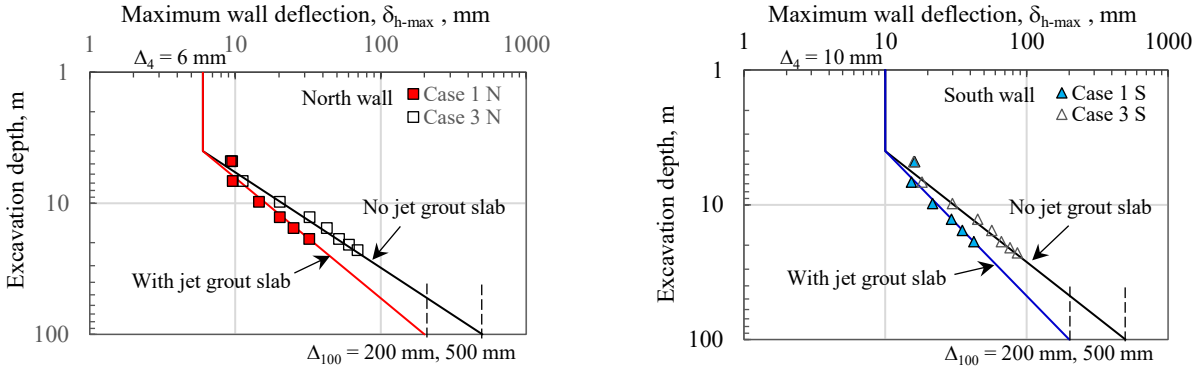

(a) North wall with piles (b) South wall with no piles

Figure 14: Effect of jet grout slab assessed by wall deflection paths - Case 1 & Case 3

6.3 Comparison between observed and computed deflection paths

The computed wall deflection paths for Case 1 are compared with those observed in the inclinometers in Figure 15. The deflection path with the set of Δ_4 and Δ_{100} values of 6 mm and 200 mm for the north side is applicable to those deflections observed in inclinometers SID4 and SIS2. For the deflections observed in inclinometers SID7 and SIS3, the set of Δ_4 and the Δ_{100} values of 10 mm and 100 mm is applicable.

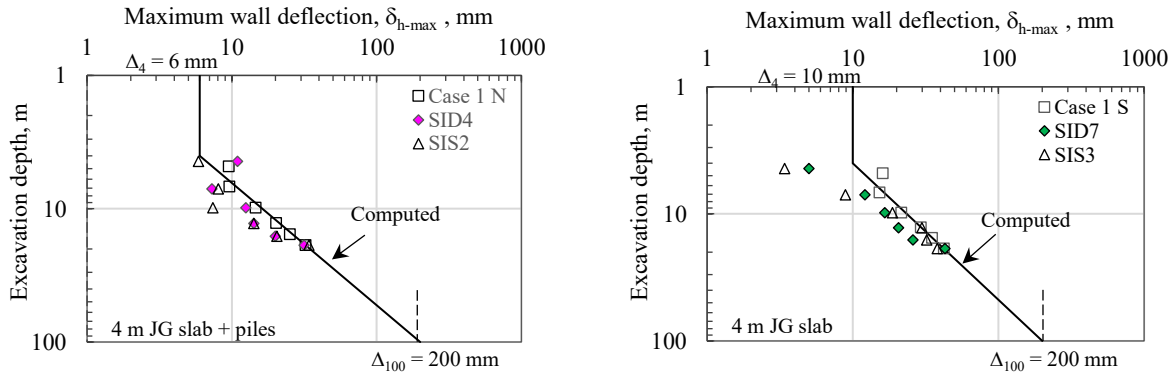

(a) North side (b) South side

Figure 15: Comparison of computed wall deflection profiles with observation - Case 1

There has been deviation on the wall deflections between the computed and the observed in the intermediate stages. In Stage 4, the observed maximum deflections deviate from the computed by 6 mm and 9 mm in the north and the south walls respectively. Such discrepancies would be due to various conditions. First of all, Chen et al. (1997) reported that traffic decks were erected along the road and jet grouting was conducted below the decks at the depth of 2.5 m. It is noted that the inclinometer readings were initialized after jet grouting at the commencement of the main excavation. The wall deflections occurred prior to the commencement of excavation were excluded. The observed wall deflection values for Stages 1 and 2 were therefore under-reported. Secondly, the utilities along the busy road were diverted on trenches of around 2 m in depth on the south side of City Hall Station. As less earth pressures acting on the south side, less wall deflections would occur. Thirdly, while drilling groutholes would disturb the soil, cement grout left in the groutholes would have some strengthening effects on the soil above the jet grout slab. Such strengthening effects have been ignored in the numerical analysis. Finally, as the excavation was conducted in thick clay layer, the consolidation effects cause delaying of the ground movements. While these various conditions have not been simulated in the analysis, discrepancies between the observed and the computed wall deflections would be inevitable.

Figure 15 shows that the observed deflections increased abruptly between Stage 5 and the final stage. The deflections in SID4 increased from 20.0 mm to 31.6 mm. In SID7, the deflections increased from 25.9 mm to 43.0 mm. As shown in Figure 12b, the horizontal strains at the interface between the north wall and the top of the jet grout slab increased from 0.68 % to 1.20 %. Such abrupt change in the rate of wall deflections is due to reaching the peak strain around 1.2 % at the top corners between the walls and the jet grout slab. Figure 15 demonstrates that the wall deflection paths is a convenient criterion that abnormal deflections such as the onset of the mobilization of the post-peak range of the jet grout slab can be identified.

7 CONCLUSIONS

Two-dimensional numerical analysis on an excavation in soft ground strengthened with jet grout slab has been conducted. The nonlinear Hardening-soil with small-strain stiffness (HSS) soil model is adopted for the soil materials. The Hardened-soil (HS) model has been adopted to simulate the nonlinear behaviour of the jet grout slab. The following conclusions could be drawn:

(1) In the estimation for the stiffness parameters for the jet grout slab, the lower bound uniaxial compressive strength and the lower bound secant modulus shall be adopted.
(2) The jet grout slab proves to be an effective method for reducing ground movements. The reduction factor could be 36 % of the excavation without jet grout slab in the final stage.
(3) The presence of the piles reduces the wall deflections by around 23 % of those without piles.
(4) The wall deflection paths interpreted from the observed and the computed wall deflections are useful criterion for assessing the performance of the wall deflections of the excavation cases. The effects of the jet grout slab and the presence of piles on the reduction in wall deflections can be readily differentiated. The wall deflection paths can identify abnormal deflections such as the mobilization of the post-peak range of the jet grout slab.

The close agreement between the computed and the observed wall deflections demonstrates that the nonlinear constitutive models for the jet grout slab and for the surrounding ground are reliable tools for analyzing the excavation works.

ACKNOWLEDGEMENTS

The Author wishes to expressed his sincere thanks to Dr R. N. Hwang of Moh and Associates, Inc. for his invaluable comments on the manuscript and in particular his advices on the assessment on the performance of the jet grout slab using the wall deflection paths.

REFERENCES

Bentley. 2022. *PLAXIS 2D-Reference Manual*. CONNECT Edition V22.02, Bentley Advancing Infrastructure, August 2022.

Benz, T. 2006. Small-strain stiffness of soils and its numerical consequence. *Dissertation of thesis*, the Institute of Geotechnics, University Stuttgart.

Chen, Y.K., Huang, C.C & Wang, F.K. 1997. Grouted raft for building protection in excavation in soft clay. *Proceedings of 7th Conference on Current Researches in Geotechnical Engineering*. Pintung, Taiwan, August, 1999: 1425-1432. (in Chinese)

Chen, Y.W., Duann, S.W., Hwang, R.N. & Kong S.K. 1999. Influence of excavation on adjacent piles. *Proceedings of 8th Conference on Current Researches in Geotechnical Engineering*. Chishan, Taiwan, August, 1997: 593-600. (in Chinese)

Chin, C.T., Chen, J.R., Hu, I.C., Yao, D.H.C. & Chao, H.C. 2007. Engineering characteristics of Taipei clay. In T.S. Tan, K.K. Phoon, D.W. Hight & S. Leroueil (Eds), entitled*: Characterization and Engineering Properties of Natural Soils,* Taylor & Francis Group, v3:1755-1803.

Chin, C.T., Crooks, A.J.H. & Moh, Z.C. 1994. Geotechnical properties of the cohesive Sungshan deposits. *Geotechnical Engineering, J. Southeast Asian Geotechnical Society*, Taipei, Taiwan 25(2): 77-103. (in Chinese)

Hwang, R. & Moh, Z.C. 2022. Groundwater drawdown and subsidence in the Taipei Basin. *Sino-Geotechnics,* No. 173/2022.9: 99-110. (in Chinese)

Hwang, R.N., Wang, C.H., Chou C.R. & Wong, L.W. 2016. Deep excavations in Taipei Basin and performance of diaphragm walls, *Geotechnical Engineering Journal of the SEAGS & AGSSEA Vol. 47, No. 2*, June 2016. ISSN 0046-5828: 34-40.

Hu. I.C., Chin, C.T. & Liu, C.J. 1996. Review of the geotechnical characteristics of the soil deposits in Taipei, *Sino-Geotechnics*, No. 54: 5-14. (in Chinese)

Kung, G.T.C, Ou, C.Y. & Juang C.H. 2009. Modelling small-strain behavior of Taipei clays for finite element analysis of braced excavations. *Computers and Geotechnics* 36 (2009): 304-319.

MAA 1987. *Engineering properties of the soil deposits in the Taipei Basin*, Report No. 85043, Ret-Ser Engineering Agency and Taipei Public Works Department, Taipei. (in Chinese)

Moh, Z.C. & Hwang, R.N. 2005. Geotechnical considerations in the design and construction of subways in urban areas. *Seminar on Recent Development om Mitigation of Natural Disasters, Urban Transportation and Construction Industry*, 30 Novmeber-2 December.

Ou, C.Y., Liao, J.T. & Cheng, W.L. 2000, Building response and ground movements induced by a deep excavation, *Geotechnique*, Vol. 50, No. 3: 209-220.

PLAXIS B.V. 2013. *PLAXIS Reference Manual*. PLAXIS, BV, Delft, the Netherlands.

Prakasa, M.D.A & Hsiung, B.C.B, 2023. Effectiveness of jet-grouted soil on excavation: A case study. *IOP Conf. Series: Earth and environmental Science*, 1249 (2023) 012022.

Santos J.A. & Correia, A.G. 2001. Reference threshold shear strain of soil. Its application to obtain a unique strain-dependent shear modulus curve for soil. *In 15th Int. Conf. SMGE*, Volume 1, Istanbul, A.A. Balkema: 267-270.

Schanz, T. & Vermeer, P.A. 1998. On the Stiffness of Sands. *Geotechnique,* 46, No. 1: 145-151.

Schanz, T., Vermeer, P.A. & Bonnier, P.G. 1999. The hardening soil model: formulation and verification. *Beyond 2000 in Computational Geotechnics*. Rotterdam, the Netherlands. 281-290.

Wong, L.W. 2024a. Ground movements caused by diaphragm wall installation. *Proceedings of the 44th HKIE Geotechnical Division Annual Seminar 2024*, May: 321-332.

Wong, L.W. 2024b. The strain-softening behaviour of jet grouted soil. *Proceedings of the HKIE-CIE-IEM Tripartite Seminar*, Hong Kong, 28 November, 2024.

Wong, L.W. & Hwang, R.N. 1997. Evaluation of Jet Grouting by In-situ Tests, *Proceedings of the International Conference on GROUND IMPROVEMENT TECHNIQUES*, May, Macau: 641-647.